Published in : The Journal of Physical Chemistry A, **2013**, *117*(51), 14267-14275.

doi.org/10.1021/jp410301d

Experimental and theoretical charge density analysis of a bromoethyl sulfonium salt.

Maqsood Ahmed[a,b], Muhammad Yar[c], Ayoub Nassour[a], Benoit Guillot[a], Claude Lecomte[a] and Christian Jelsch[a]

[a]*CRM2, CNRS - Institut Jean Barriol. Université de Lorraine, Vandoeuvre-lès-Nancy, France*

[b]*Department of Chemistry, The Islamia University of Bahawalpur, Pakistan.*

[b]*Interdisciplinary Research Center in Biomedical Materials, COMSATS Institute of Information Technology, 54000, Lahore, Pakistan.*

Correspondence: christian.jelsch@univ-lorraine.fr

Abstract

Bromoethyl sulfonium trifluoromethanesulfonate is a salt complex in which a sulphur atom makes three covalent bonds. This molecule has been proved to act as an efficient annulation reagent which results in the formation of synthetically challenging and pharmaceutically important 4-, 5-, 6- and 7-membered heterocycles in excellent yields. The charge density of the molecule was determined from both experimentally and theoretically derived diffraction data. The stereochemistry and electron density topology of the sulfonium group was analysed. To understand the chemical reactivity of the molecule, the electrostatic potential difference between the two carbon atoms of the bromoethyl group was investigated. It has been considered that the hydrogen atoms on the carbon atom bound to sulphur are more acidic in character due to their vicinity with the triply covalently bonded positively charged sulphur atom. The electropositivity of the S-attached and Br-attached methylene groups are compared in the experimental and theoretical charge densities using topological atomic charges and electrostatic potential at the molecular surface.

Keywords. Electron density. Electrostatic potential. Nucleophile, Chemical reaction.

Introduction.

Bromoethyl sulfonium triflate **1 (**or BEST, Scheme 1) has been found to be an effective annulation reagent in the synthesis of various medicinally important compounds[1-7]. Diphenylvinylsulfonium triflate **2** (or DVST, Scheme 1) has been extensively used and found to be very reactive towards various nucleophiles. A variety of nitrogen, sulphur, oxygen, and carbon-based nucleophile molecules undergo conjugate addition to vinyl sulfonium salts in the presence of base[3,5,8] the resulting ylide have two possible reaction pathways depending upon the substrates type. In a first reaction type, the resulting ylides can be trapped intra or intermolecularly by aldehydes or imines to produce epoxides or aziridines respectively[1,2,5,9]. In another reaction type, ylides undergo intramolecular proton transfer from an acidic site and the anion generated then displaces the sulfide to effect a ring-closure to generate required heterocycles[7,10].

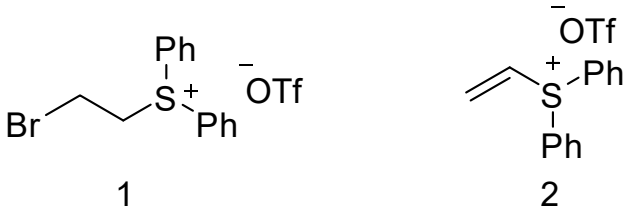

Scheme 1: Chemical diagram of bromoethyl sulfonium trifluoromethanesulfonate 1 (BEST) and diphenylvinylsulfonium triflate 2 (DVST)

DVST is good alternative of 1, 2-dihaloethanes for the synthesis of heterocycles. 1, 2-dihalo derivatives tend to be poorer electrophile groups and their reactions are often accompanied by competing elimination processes. For example, the direct synthesis of 1,4-diheterocyclic compounds by alkylation of β-amino alcohols/thiols/amines with 1,2-dihaloethanes often gives low yields and side reactions[11]. DVST (soft electrophile, good Michael acceptor) operates under less basic conditions and minimizes competing elimination pathways. Thus, the efficient synthetic procedure for DVST and its synthetic applications has made it an attractive annulation agent.

It was later discovered that these annulations can be indeed conducted using BEST compound **2** which possibly generates diphenylvinylsulfonium triflate *in situ*. BEST is a crystalline solid and is easier to handle and store as compared to free flowing oil DVST[4]. BEST works effectively with a modification of the nature of the base; this method gave access to a range of

heterocycles in high yields (Scheme 2). The range of nitrogen substituents demonstrated to be suitable was expanded to include sulfinamides, *N*-aromatics and *N*-heteroaromatic substituents[4,6]. Concerning the challenging synthesis of seven-membered heterocycles (diazepines and oxazepines), the annulation reaction of 1,3-aminoalcohols and 1,3-diamines with BEST gave 7-membered ring heterocycles in good yield[4]. Employing *N*-tosyl 1, 3-amino alcohols or 1, 3-diamines and bromoethyl sulfonium salt yielded 1, 4-oxazepines or 1, 4-diazepines respectively in moderate-to-excellent yields. A mixed *N*-tosyl/*N*-SES 1, 3-diamine gave a heterocycle bearing orthogonally protected amines which can be deprotected and derivatized as required.

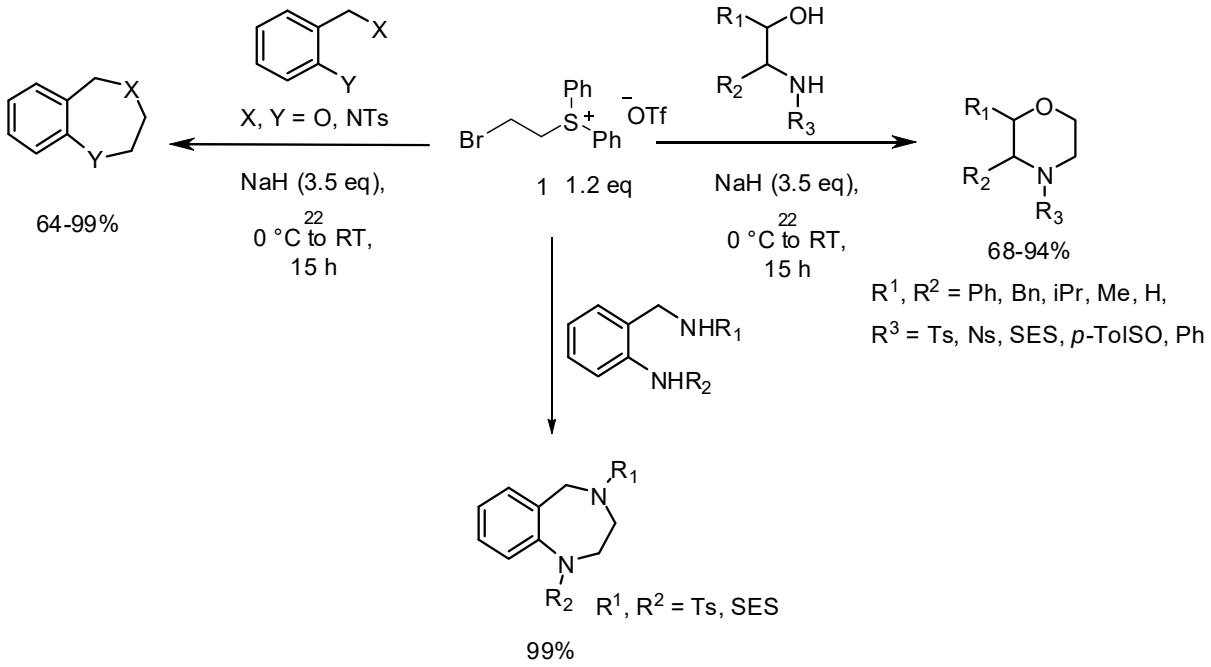

Scheme 2: Schematic illustration of reactions involving BEST to give various heterocycles.

When BEST is employed in the transformations described above, one can draw a plausible mechanism involving successive SN^2 displacements of diphenylsulfide and bromide. It has been suggested that the reaction proceeds through *in situ* formation of DVST followed by conjugate addition as shown in Scheme 3[1-5].

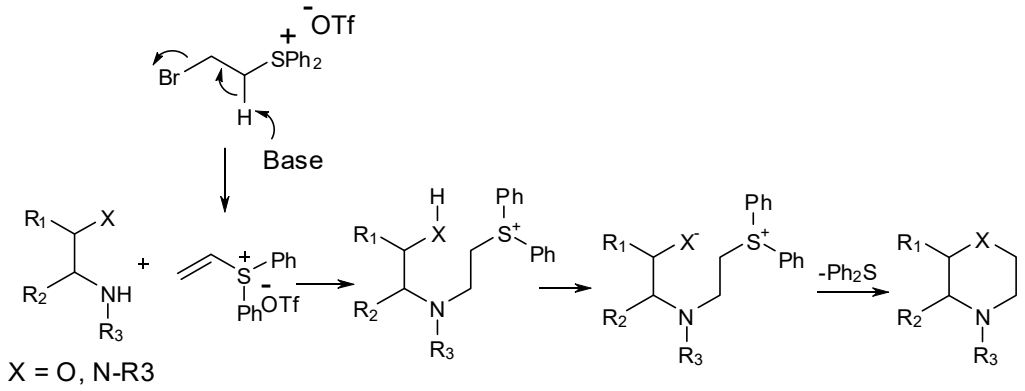

Scheme 3: The reported proposed mechanism of annulation reaction involving BEST (see references above)

As the reactivity of a compound such as BEST is related to its electron distribution, a precise charge density analysis (either experimental or theoretical) is a method of choice to recover molecular properties. In particular, it is of interest to know how the two CH_2 carbon units present in compound BEST between the bromine and the sulphur atom are different from a charge distribution point of view. It has been assumed[4], that the carbon atom attached to the sulphur atom is probably more electron deficient due to the positive charge of S and hence would be the site of attack by a base, owing to its comparatively acidic hydrogen atoms (Scheme 4).

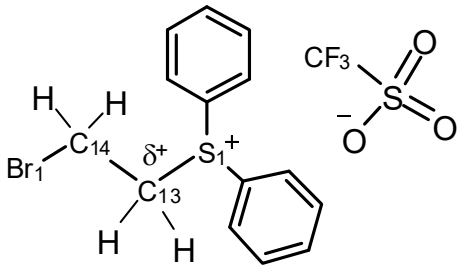

Scheme 4: The proposed[4] distribution of charges on C13 and C14 atoms in BEST compound.

To test this hypothesis, an experimental (Exp) and theoretical (Theo) charge density determination bromoethyl sulfonium trifluoromethanesulfonate **1** (BEST) was carried out.

Materials and Methods.

Crystallization.

The synthesis of the BEST compound was described before[3-5,12]. Being an organic salt, the compound crystallizes very easily in a number of solvents including alcohols, acetone, and chloroform. For the current experiment, the crystals were grown by –slow evaporation of a toluene solution of BEST compound in a few days at room temperature. A single, colorless crystal of dimensions 0.18×0.16×0.15 mm was selected for the diffraction experiment.

Data Collection

Single crystal X-rays high resolution and highly redundant data collection of BEST was performed on an *Oxford SuperNova*[13] diffractometer using Mo Kα radiation (λ = 0.71073 Å). Details of data collection and refinement procedure are given in Table 1. The crystal was mounted on a glass needle using silicone greasFige and cooled from room temperature to 100(1) K over a period of one hour under a stream of liquid nitrogen using the Oxford Cryo-systems gas flow apparatus. The *SuperNova* diffractometer works under the software *CrysAlisPro*[13] which calculates the strategy to optimize the angular positions of detector and the goniometer head during the data collection.

Table 1: Crystal and data collection statistics.

Chemical formula	C_{15} H_{14} Br F_3 O_3 S_2
Molecular weight (g/mol)	443.29
Space group	Monoclinic $P2_1/n$
Temperature (K)	100 (1)
a , *b*, *c* (Å)	11.7897(8), 10.5840(6), 13.6153(6)
β (°)	97.989(10)
Radiation type	Mo *Kα*
Crystal shape	Prism, colorless
Crystal dimensions (mm)	0.18×0.16×0.15
Diffractometer	' Oxford SuperNova'
Absorption correction	Analytical (Clark & Reid, 1995)
μ (mm^{-1})	2.737
T_{min}, T_{max}	0.648, 0.795
$\sin\theta_{max} / \lambda$	1.02

# measured, independent	679 441, 15 489
# used reflections	14 538 ($I > 0\sigma$)
Completeness (%)	99.9
R_{int} % / Redundancy	5.7 / 35

A first diffraction data set was collected under ω scans of 1° intervals. To improve the quality of the data, a second data set was later collected using the same crystal at the same temperature, but using different exposure times in the experiment. In the first experiment, the exposure time was 10 s and 25s for low high resolution data. In the second experiment, a 45s exposure time was used for high angle data collection whereas the low angle data were also collected at the 10 s exposure time. The image frames were indexed and integrated using *CrysalisPro* package. An analytical absorption correction[14] was applied on the basis of the face indexes of the crystal. The Friedel mates were merged during data processing, the crystal being centrosymmetric space group $P2_1/n$. The two data sets were then merged using *SORTAV*[15]. Although intensity peaks were observed up to d=0.44Å resolution, the data resolution was truncated at d>0.50Å as the very high resolution reflections were very weak and the $<I_{obs}>/<I_{calc}>$ ratio became significantly larger than unity (reaching 1.16) as verified with *XDRKplot*[16] software (see supplementary materials).

Structure solution and refinement

The structure was solved in the monoclinic $P2_1/n$ space group using the *SIR92*[17] software. An initial Independent Atom Model (IAM) refinement was undertaken using the *SHELXL97* software[18]. The model was subsequently imported to *MoPro*[19] software. The hydrogen atom positions were constrained to the standard neutron distances as available in the International Tables of Crystallography[21]. The bromine atom was modelled using an anharmonic thermal motion description up to fourth order of Gram-Charlier parameters, the resulting (root mean square)/<sigma> ratio is 7.0. An *ORTEP*[22] diagram of the molecule showing the atom numbering scheme and thermal ellipsoids is shown in Fig. 1.

Figure 1. *ORTEP* diagram of the molecule showing the atom numbering scheme and the thermal displacement ellipsoids, drawn at 50% probability level.

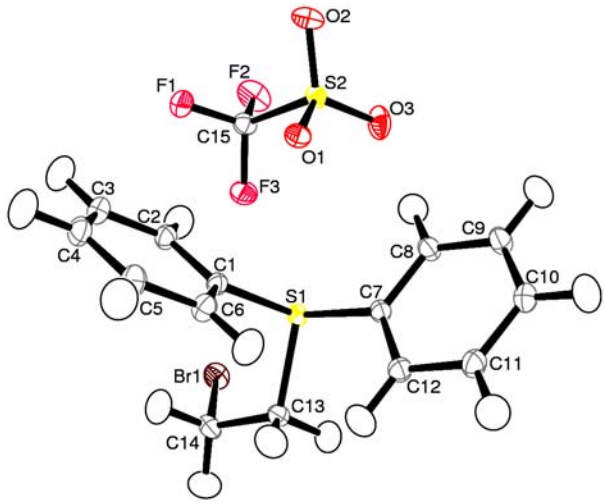

The Fourier residual electron density maps obtained after the experimental IAM refinement are shown in Supplementary Materials. Examination of these maps demonstrate the quality of the experimental data, as deformation bonding electron densities can be found on all covalent bonds, as well as around atoms holding electron lone pairs (S, Br). The crystallographic statistics are given in Table 2.

Table 2: Crystallographic agreement factors and residual electron density values obtained after multipolar refinements of the BEST molecule.

Data	EXP	DFT DZP
Resolution (Å)	0.50	0.40
$R(F)$ %	1.68	1.10
$wR_2(F)$ %	1.15	1.07
G. o. f	0.99	/
$\Delta\rho_{max}$ (e/Å^3)	0.36,	
$\Delta\rho_{min}$	-0.41	
$\Delta\rho_{rms}$	0.055	

Experimental multipolar refinement

The least squares multipole refinement was carried out with MoPro software[19] on the basis of Hansen & Coppens[20] model. The parameters of the Slater radial functions used for the multipolar description of atoms are given in Table Sup3. Reflections up to d=0.50Å resolution and with I>3sigma were used in the refinement. The different structural and charge density

parameters were refined iteratively. The coordinates and thermal displacement parameters of all non-hydrogen atoms were refined using high-order diffraction data only (d<0.7Å) in the initial stages of the refinement. After a first round of charge density refinement, the anisotropic thermal displacement parameters of H atoms were calculated with the *SHADE* server[29] and were kept fixed subsequently.

Constraints and restraints.

The C-H covalent bonds were restrained to standard neutron distances[21] (σ_d=0.002Å). The target C-H distances were 1.083(2) for aromatic groups, 1.059(2) for the bromomethyl group and 1.092(2) Å for the methylene group.

The following restraints were applied in the experimental charge density refinement. The κ parameters of all the H atoms were restrained to 1.16 (0.01)[30].

R-free refinements were performed to estimate the best weight to be applied to the chemical equivalence and multipoles local symmetry restraints[31]. The sigma value σ_r=0.02 was found to be optimal as it gave the lowest values of $wR^2(F)$ free factor (Fig. Sup4). A mirror symmetry restraint was imposed on the S1 atom as it is linked to two sp^2 and one sp^3 carbon atoms. A *3m* symmetry restraint was imposed on the triflate S2 atom (C-SO_3^- type) (see Fig. 1**)**. Similarly *3m* symmetry was imposed on atom C15 bearing the three fluorine atoms. All other carbon atoms had one single mirror symmetry. The charge density parameters of the chemically equivalent atoms were restrained to be similar with the same sigma value σ_r. The two ions forming the asymmetric unit were constraint to have a formal charge of ±1.

It was observed that the multipolar refinement did not allow reaching a proper charge distribution model for the three fluorine and oxygen atoms of the triflate anion. This was probably due to the higher thermal motion within the triflate which has a rotation degree of freedom around the S-C axis, the F2 atom has a U_{eq} value reaching 0.03 Å^2. Chemical equivalence constraints were therefore applied to the three fluorine and oxygen atoms, which yielded realistic experimental deformation electron density.

At the end of the multipolar refinement against the experimental data, the R (F) factor was 1.68 % and the *goodness of fit* was 0.99. All the fractional coordinates, bonds lengths, bond angles and thermal displacement parameters are listed in the CIF file, in Supplementary Materials.

Theoretical calculations

CRYSTAL09[22] program package was used to perform periodic quantum mechanical calculations. The crystal geometry observed experimentally was used as a starting geometry and optimization of the hydrogen atom positions was performed with density functional theory (DFT) method[23] and with the B3LYP hybrid functional[24,25] using 6-31G (*d,p*) basis set[27]. Upon convergence on energy ($\Delta E \sim 10^{-6}$), the periodic wave function based on the optimized geometry was obtained. The index generation scheme proposed by Le Page & Gabe[28]was applied to generate 27 520 unique Miller indices up to $\sin\theta/\lambda$ = 1.25 $Å^{-1}$. The option XFAC of the CRYSTAL09 program was then used to generate a set of theoretical structure factors from the computed electron density using the set of prepared indices.

Structure factors were calculated and were taken as observed data set in a subsequent refinement of the charge density parameters with the software MoPro. For the non-H atoms, a κ coefficient applying to the core electron density was in addition refined, as performed previously in a charge density analysis of corrundum[32]

Results and Discussions

Electron density

Some static deformation and the corresponding residual electron density maps obtained at the end of the multipole refinement against experimental data are shown in Supplementary Materials. The Fourier residual electron density maps are almost featureless (Table 2). A three dimensional view of the static deformation electron density around the S1 atom is shown in Fig. 2. An electron lone pair is visible on the S1 sulphur atom and forms a tetrahedral geometry with the three C-S bonds. The sulfonate S2 atom of the triflate anion has a different configuration as it is bonded with three oxygen atoms and one carbon atom and is arranged in a nearly tetrahedral geometry (Fig. 1).

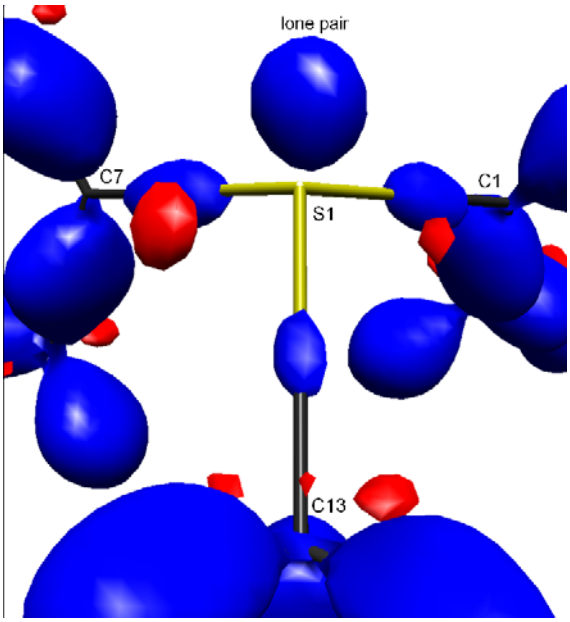

Figure 2. 3D view of the experimental static deformation electron density showing the electron lone pair of the sulphur atom. Blue colour shows deformation electron density accumulation and red colour shows the depletion. Isosurfaces levels are ±0.2 eÅ^{-3}.

Bond Critical points.

The covalent bond critical points (BCP) were searched and are shown in Fig. 3 while the topological properties are listed in Table 3 and Sup1. It can be observed in Table Sup1 that the topological values from experiment and theory are in general agreement with each other.

Figure 3: The covalent bond critical points shown in dark brown colour for the experimental model.

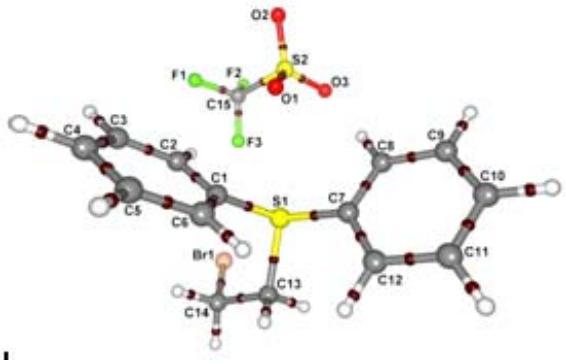

Table 3: Topological properties at the bond critical points in the bromoethyl-sulfonium and triflate parts of the BEST molecule (experimental multipolar model). d_{12} is the interatomic distance, d_{1cp} and d_{2cp} (Å) is the distance between the first / second atom and the CP; $\rho(r_{cp})$ is the total electron density (e.Å^{-3}); $\nabla^2\rho(r_{cp})$ is the Laplacian (e.Å^{-5}) and ε the ellipticity. The values are from the experimental model. Other BCPs and values from theory are described in supplementary materials.

Bond	d_{12}	d_{1cp}	d_{2cp}	$\rho(\mathbf{r}_{cp})$	$\nabla^2\rho(\mathbf{r}_{cp})$	ε
BR1-C14	1.9458(6)	1.0948	0.8513	0.9662	0.03	0.01
S1-C1	1.7823(5)	0.9493	0.8330	1.2739	-5.7	0.05
S1-C7	1.7796(5)	0.9508	0.8291	1.2880	-5.5	0.04
S1-C13	1.8158(5)	0.9785	0.8372	1.1891	-4.5	0.08
C13-C14	1.5126(7)	0.7855	0.7278	1.6641	-10.2	0.04
C13-H13A	1.0907	0.7393	0.3515	1.7932	-15.9	0.00
C13-H13B	1.0914	0.7309	0.3606	1.7418	-14.9	0.00
C14-H14A	1.0914	0.7338	0.3577	1.8048	-16.5	0.01
C14-H14B	1.0919	0.7308	0.3611	1.7789	-15.9	0.01
S2-C15	1.8320(6)	0.8981	0.9341	1.3348	-9.2	0.02
S2-O1	1.4508(8)	0.5918	0.8591	2.1894	3.3	0.06
S2-O2	1.4467(9)	0.5921	0.8552	2.1741	3.8	0.01
S2-O3	1.4410(9)	0.5924	0.8503	2.2165	3.8	0.01
F1-C15	1.3415(6)	0.8238	0.5180	1.9470	-15.6	0.05
F2-C15	1.3334(7)	0.8263	0.5074	1.9328	-13.9	0.06
F3-C15	1.3340(6)	0.8236	0.5109	1.9784	-16.2	0.07

The $\nabla^2\rho_{cp}$ values of the Laplacian at the BCPs are found to be negative except on the sulfonate S-O bonds and on the C-Br bond. This is the case for both experimental and theoretical cases and denotes the polar character of these bonds. A negative minimum of the Laplacian is however found on the C-O bond path to the oxygen atoms and on the C-Br bond closer to the electronegative Br atom (Fig. 4). The values of the ellipticity on the S-O bonds are small (0.03±3 on average) and reflect the nearly three-fold symmetry character of the O-SO_2C bonds; the three S-O distances are very similar 1.446±5Å.

The negative Laplacian is stronger on the triflate S2-C15 BCP than on the S1-C BCPs of the sulfonium, despite a longer bond length for S2-C15 (1.8320(5)Å *vs* 1.79±2 Å). The same tendency is observed for the Theo charge density. Contrarily to non-polar bonds, the Laplacian $\nabla^2\rho_{cp}$ cannot be directly related to the bond strength in polar bonds such as S-C or S-O. This result can be related to the experimental charge density study of K_2 sulphate[34], where the longest S-O bonds have also the strongest $\nabla^2\rho_{cp}$ Laplacian values. When the S−O distance is decreased in sulphate, the S−O bond unexpectedly becomes less covalent because of a counterbalancing effect arising from the large enhancement of the bond polarity. In theoretical studies of S-O and N-O polar covalent bonds in several small molecules *in vacuo*, Love[35,36]

found however that the Laplacian $\nabla^2\rho_{cp}$ is generally decreasing in magnitude when the bond length increases.

It can also be noticed that the BCP is closer to the carbon atom in the sulfonium C-S bonds while the reverse occurs in the triflate C-S bond, denoting the stronger electron depletion of the sulfonate S atom. The three sulfonium S-C bonds have ellipticities of 0.06±2 and the S1-C13 bond involving a sp^3 C atom is slightly longer than the two others which involve aromatic C atoms (Table 3).

Figure 4. Electron density Laplacian $\nabla^2\rho$ maps of the experimental multipolar model**.**

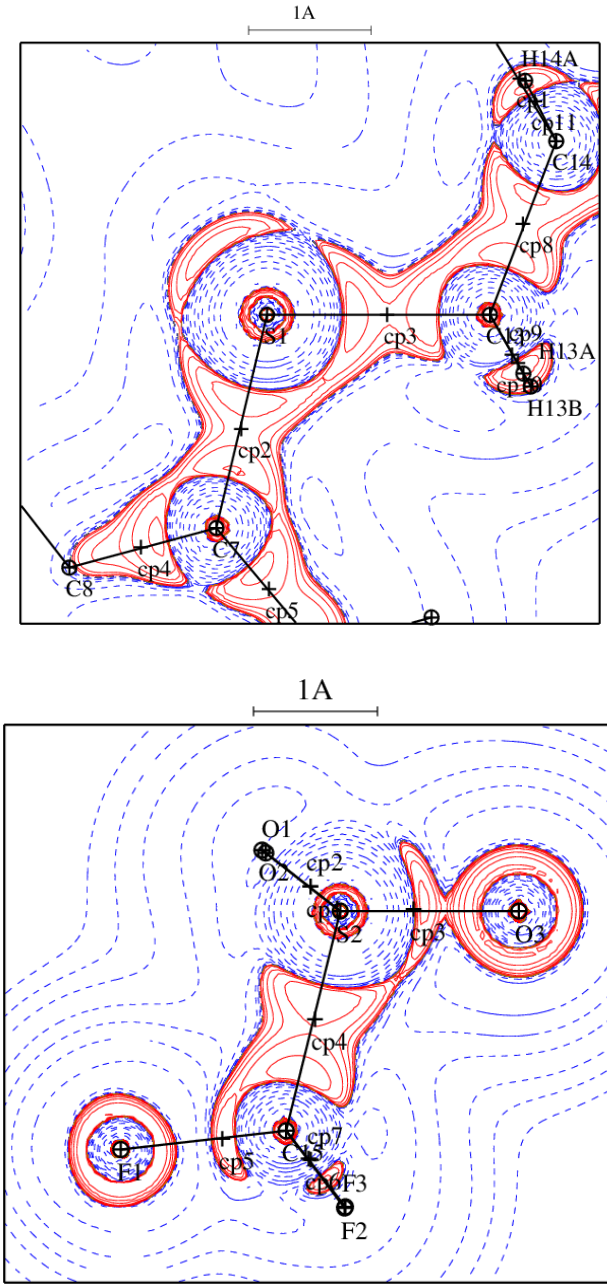

(a) in the C14-S1-C7 sulfonium plane

(b) in the C15-S2-O3 plane of the triflate anion.

The values of ellipticity for the aromatic $C(sp^2)$-$C(sp^2)$ bonds on the phenyl rings are higher which is related to the partial double bond character. The average value is ε=0.20±2 and 0.16±2 for the twelve C-C covalent bonds found in the two phenyl rings, for the Exp and Theo models, respectively.

Intermolecular interactions.

There is a large number of intermolecular interactions of different nature present in the crystal structure. The Hirshfeld surface analysis was performed with program CRYSTALEXPLORER[38] to find out the respective proportions of the various interactions. A Hirshfeld surface[39] of the molecule (Fig. Sup6) shows the areas where intermolecular interactions are shorter than the sum of atomic van der Waals radii.

The 'fingerprint' plots of the interactions are shown in Supplementary Materials and a breakdown of the interaction surfaces is listed in Table 4. The H···O hydrogen bonds constitute the largest contact area, followed by H···H, H···F and H···C interactions. The H···Br interactions are present in a significant ratio of 10.6%. A small but interesting proportion of interactions of Br···F type is also observed although the bromine and the F2 atoms are distant by more than 3.45Å in the crystal packing.

Table 4: Breakdown of the most prevalent (>1%) intermolecular interactions in the BEST crystal packing with their respective proportions:

contacts	%	contacts	%
H···O	23.2	H···Br	10.6
H···H	20.8	C...F	6.7
H···F	19.5	Br...F	1.7
H···C	14.3	C...O	1.5

A topological analysis of the total electron density in the intermolecular interactions regions on the basis of Bader theory[35] of "Atoms In Molecules" (AIM) is a very informative way to study the nature of interactions. A topological analysis was performed for all the significant and weak interactions in the crystal packing and the intermolecular CPs were located. The topological values for all the (3,-1) type interactions are listed in Table Sup2.

There are only C-H···O type hydrogen bonds in the crystal packing of BEST compound and those with H···O distance significantly below the van der Waals contact distance are reported in Table 5. The topological values reveal that some of the interactions are remarkably strong. For example, the O3^{i}···H13A-C13 hydrogen bond has very high electron density and Laplacian values at the CP. The 2.155 Å O···H distance (Exp model) is quite short for a C-H···O type weak hydrogen bond[38] and represents a significant interpenetration of atoms beneath van der Waals contact (d = 2.61 Å). The oxygen atom O3 on the $–SO_3^-$ group is a strong acceptor, while H-bonds are shorter when the H-C donors are acidic; this is the case for H13A as its electrons are withdrawn by the nearby sulfonium atom.

Table 5: Selection of hydrogen bonds and their topological properties at the CP for the experimental model. Definitions are in Table 3. *G* and *V* are the kinetic and potential energy density at the CP (kJ/mol/bohr^3). The symmetry codes are the:
(i) *X ; Y-1 ; Z* (ii) *-X+1 ; -Y ; -Z+1* (iii) *X+½ ; -Y-½ ; Z-½* (iv) *-X+3/2 ; Y-½ ; -Z+3/2*
(v) *X- ½ ; -Y-½ ; Z-1/2* (vi) *X+½ ; -Y-½ ; Z-½*

Bond Path	d_{12}	d_{1cp}	d_{2cp}	ρ	$\nabla^2\rho$	ε	G	V
O1···H6 (iv)	2.396	1.465	0.969	0.068	1.08	0.43	23.1	-16.9
O1···H13B (iv)	2.738	1.625	1.130	0.021	0.44	0.37	8.4	-4.95
O1···H12 (iv)	2.311	1.403	0.932	0.066	1.17	0.01	24.7	-17.4
O2···H4 (v)	2.661	1.539	1.164	0.042	0.63	0.13	13.0	-8.87
O2···H10 (iii)	2.692	1.617	1.085	0.021	0.48	0.16	9.2	-5.53
O2···H14B (i)	2.483	1.469	1.037	0.044	0.77	0.06	15.7	-10.4
O3···H13A (ii)	2.151	1.290	0.877	0.107	1.72	0.03	38.8	-30.8
F2···H9 (vi)	2.675	1.495	1.210	0.027	0.48	0.27	9.5	-5.88
F1···H10 (vi)	2.667	1.480	1.212	0.037	0.62	0.07	12.5	-8.19

The sulfonium S1 atom shows no intermolecular CP, although it is in contact with the sulfonate O3 atom at a 3.169(1) Å, which is a distance below the van der Waals contact.
There 5, 6 and 7 critical points related respectively to H···H, H···F and H···C interactions (Table Sup2).

Atomic charges

On the basis of the multipolar refinement result, an analysis of the valence populations was made, as atomic charges can be derived from them. The kappa refinement formalism[33] was considered to avoid the possible charge transfers between atoms due to the multipoles in the

Hansen & Coppens modelling. The valence populations P_{val_κ} results of the kappa refinements are mentioned in Table 6.

Table 6. Valence populations P_{val_κ} derived from the kappa refinements and P_{AIM} derived from topology, using experimental (Exp) and theoretical (Theo) models (e). $P_{AIM} = Q_{AIM} - N_{cor}$ is the number of electrons Q_{AIM} integrated over the Bader atomic basins (multipolar models) minus N_{cor}, the number of core electrons. Atomic charges can be retrieved by difference N_{val}-P_{val} with the number of valence electrons N_{val} of the neutral atom. N_{val} = 7, 6, 7, 6, 4, 1e for Br, S, F, O, C and H respectively and $N_{val} + N_{cor} = Z$, the atomic number.

Atom	P_{val_κ} Exp	P_{AIM} Exp	P_{val_κ} Theo	P_{AIM} Theo	Atom	P_{val_κ} Exp	P_{AIM} Exp	P_{val_κ} Theo	P_{AIM} Theo
F1	7.11(2)	7.58	7.22(1)	7.57	Br1	6.57(8)	7.04	7.37(3)	7.44
F2	=F1	7.57	7.22(1)	7.61	O1	6.48(2)	7.27	6.53(1)	7.33
F3	=F1	7.59	7.22(1)	7.62	O2	=O1	7.27	6.53(1)	7.31
S1	5.38(6)	5.50	5.62(3)	5.69	O3	=O1	7.26	6.53(1)	7.35
S2	5.50(7)	2.86	5.25(3)	2.26	C8	4.23(6)	4.04	4.15(3)	3.92
C1	4.26(6)	4.14	4.10(3)	4.11	C9	4.21(7)	4.09	4.14(3)	3.95
C2	4.34(6)	4.03	4.18(3)	3.89	C10	4.21(6)	4.15	4.16(3)	3.97
C3	4.17(7)	4.09	4.19(3)	3.96	C11	4.08(7)	4.13	4.18(3)	3.92
C4	4.28(6)	4.23	4.17(3)	3.96	C12	4.27(6)	4.03	4.12(3)	3.91
C5	4.21(7)	4.04	4.17(3)	3.94	**C13**	**4.20(6)**	**4.24**	**4.35(3)**	**3.96**
C6	4.16(6)	4.12	4.19(3)	3.94	**C14**	**4.41(7)**	**4.13**	**4.12(3)**	**3.92**
C7	4.16(6)	4.14	4.10(3)	4.10	C15	3.73(6)	2.59	3.48(2)	2.96
H2	0.77(2)	0.86	0.77(1)	0.99	H10	0.77(2)	0.87	0.78(1)	0.95
H3	0.80(2)	0.85	0.78(1)	0.97	H11	0.83(2)	0.86	0.76(1)	0.97
H4	0.75(2)	0.83	0.77(1)	0.93	H12	0.79(2)	0.80	0.77(1)	0.97
H5	0.78(2)	0.85	0.76(1)	0.95	**H13A**	**0.81(2)**	**0.83**	**0.74(1)**	**0.93**
H6	0.75(2)	0.82	0.76(1)	0.98	**H13B**	**0.79(2)**	**0.86**	**0.75(1)**	**0.96**
H8	0.74(2)	0.85	0.76(1)	0.97	**H14A**	**0.77(2)**	**0.84**	**0.77(1)**	**0.94**
H9	0.77(2)	0.87	0.76(1)	0.99	**H14B**	**0.74(2)**	**0.85**	**0.76(1)**	**0.90**
			Methylene Charge		**C13**	+0.20	+0.06	+0.16	+0.15
					C14	+0.08	+0.18	+0.35	+0.24

The Bader Quantum Theory of Atoms in the Molecules (QTAIM)[34] provides another reliable method to calculate atomic charges on the basis of the total electron density only. It is based on a topological analysis of the total electron density to provide bond topological properties but also atomic properties like charges, volumes and de-localization indexes used to find the bond-order of the reactive surfaces delineating regions of charge concentration from charge depletion[37]. The Q_{AIM} charges were integrated for a promolecule using the VMoPro software[19].

The charges on the two sulphur atoms are worth comparing. The S1 atom has three covalent bonds and has a positive topological Q_{AIM_EXP} charge of +0.50e. The sulfonate S2 atom in the triflate anion is bonded to three oxygen atoms and has three fluorine atoms as its second neighbours. This position of S2 renders it highly deficient in electrons resulting in a net integrated Exp charge largely positive of +3.14e. The three oxygen atoms display similar S-O bond lengths 1.446±0.004Å. Their three atomic charges, which were not constrained to be equivalent in the Theo model, are similar. The cumulative negative Q_{AIM_EXP} charge on the three oxygen atoms riding on S2 atom is -3.80e (1.26 each as they were constraint to be equivalent) while that on the three fluorine atoms is -1.74 e.
The C15 atom holding the three fluorine atoms bears a large positive charge (Q_{AIM_EXP} =+1.41e). For the two charge definitions and the two models, this carbon atom is positively charged, while the fluorine atoms are negatively charged for all charge definitions.
The charge values of atoms in the triflate moiety are larger for the Q_{AIM} definition than for the Q_{val_κ} one.

In order to analyse the important role of the bromoethyl hydrogen atoms in the proposed mechanism, the charges of C13 and C14 atoms and those of their bonded hydrogen atoms deserve special attention. The C13 methylene CH_2 group was found to bear globally a slightly less positive charge compared to the C14 methylene for three out of the four charge types given in Table 6, presumably due to the presence of a bromine atom bound to C14 vs. a sulfonium on C13 atom. The relative acidity of H14(A,B) vs. H13(A,B) atoms varies with the charges model considered.
The bromine atom is negatively charged in three charge models, except for Q_{AIM_EXP}. The possible charge distribution of atoms mainly involved in the reaction mechanism, represented in Scheme 10, is compatible with the same three types of charges.

Scheme 10: Distribution of charges in the light of charge density analysis.

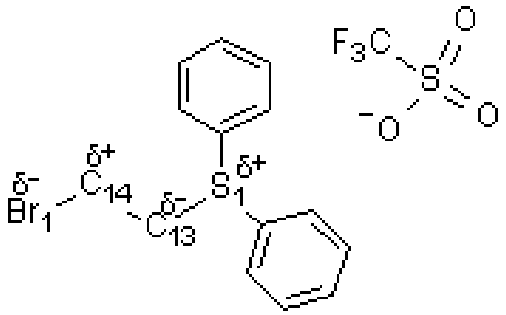

A refinement with the charges of the anion and cation not constrained to a formal unitary charge was also performed. The asymmetric unit having been kept neutral electrically during the refinement, the two ionic moieties necessarily hold complementary charges. The resulting model should reflect the ionic character of both molecules in the asymmetric unit. This is indeed the case, the triflate moiety turns out to be significantly negative as the sum of its atomic valence populations led to a total charge of -0.84 e in the Exp model, while the Theo charge -0.62e is more attenuated.

Electrostatic Potential

As the BEST compound is an ion pair, the triflate molecule has an overall negative electrostatic potential (ESP) and the bromoethyl biphenyl sulphonium moiety has an overall positive ESP. The electron density surface coloured according to the ESP is shown in the Fig. 5. Globally, the Exp ESP shows larger values compared to the ESP derived from the Theo model. A large area of positive ESP is observed around the sulfonium group in both cases. The positive ESP generated by the sulphur atom is propagated towards the hydrogen atoms of the reactive bromoethyl group in the theoretical ESP.

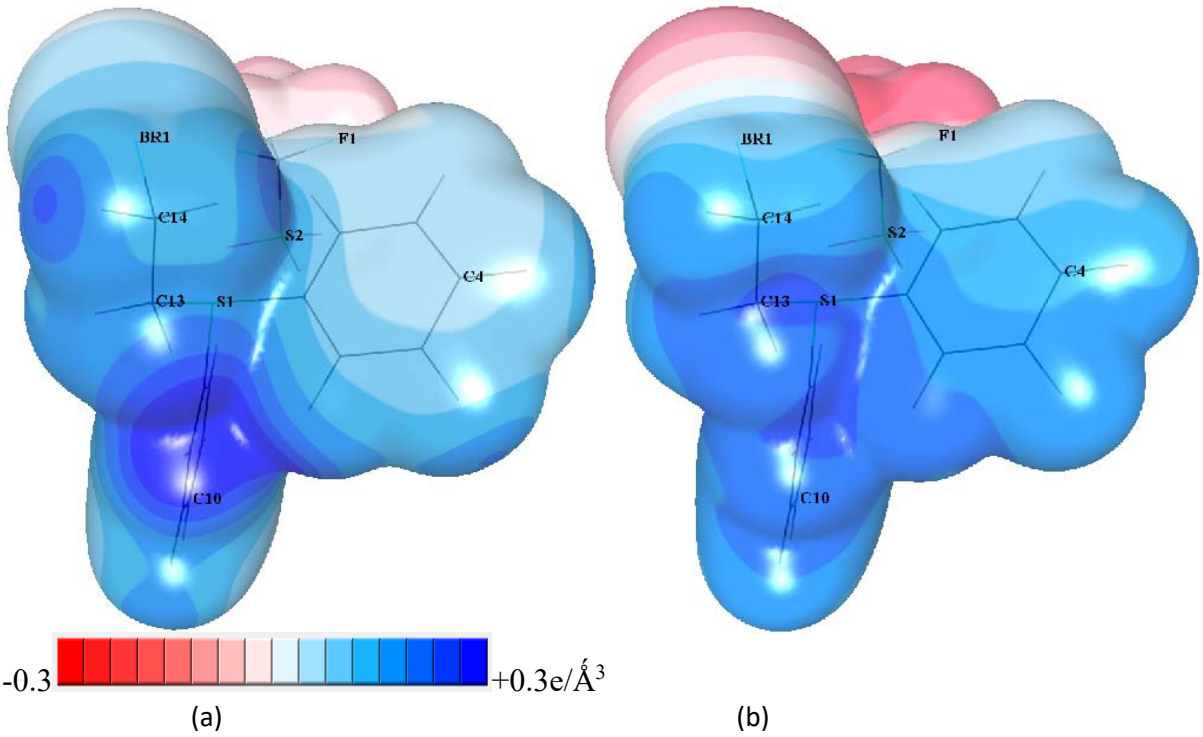

Figure 5. Isosurface of static total electron density at ρ=0.01 e/Å^3 coloured according to the electrostatic potential generated by the BEST promolecule. The bromoethyl sulfonium moiety is in the foreground while the negatively charged triflate group is behind. The view highlights the difference between the H atoms bound to C13 and C14 atoms. Properties are computed using (a) experimental data (b) theoretical multipolar model.

The ESP issued from the Exp multipolar refinement is more positive around the two H14A,B hydrogen atoms (Fig. 5), due to more positive charges on the hydrogen atoms and on the bromine atom. The converse is observed for the theoretical model, where the potential is more positive around the H13A,B atoms due to the influence of the vicinal positive sulfonium atom. The electrostatic potential is much more electronegative in the theoretical model on the bromine atom compared to the experimental one.

The isosurface coloured according to the ESP issued from the refinements without formal ±1e charge constraint on the cation/anion pair is shown in Fig. Sup7. The unconstrained Exp electrostatic potential is slightly attenuated compared to the constrained one, as the charge transfer between the ions is lower, but is qualitatively similar to the constrained one, notably around the bromoethyl group. The ESP from the theoretical unconstrained model is also attenuated except for the bromine atom and the region around which is far more electronegative.

Dipole moment.

The molecular dipole moments **μ** are calculated, based on atomic net charges q_i derived from P_{val} and on the atomic dipoles μ_i (from the multipole formalism), according to the formula:

$$\vec{\mu}_{Total} = \sum_i \vec{\mu}_i + \sum q_i \vec{r}_i$$

Due to the electroneutrality constraint which kept the total charge of the asymmetric unit equal to zero, **μ** is actually independent of the origin. The atomic dipole moment contributions are dependent on seven variables: the net charge derived from P_{val}, the atomic coordinates (corresponding to the location in space of atomic charges) and the three dipole populations P_{10}, P_{11+}, P_{11-}.

The BEST salt compound, being a polar entity, possesses relatively high dipole moment, which is found to be 25.2 D and 28.8 D for the Exp and Theo models, respectively. The dipole moment vectors are shown in the Fig. 6 for both models. The system being composed of anionic and cationic molecules, the dipole moment orientation and magnitude is largely ruled by this property. Hence the dipole moments vectors are roughly oriented in the direction joining the negative triflate moiety to the positive region located next to the C13-C14 group.

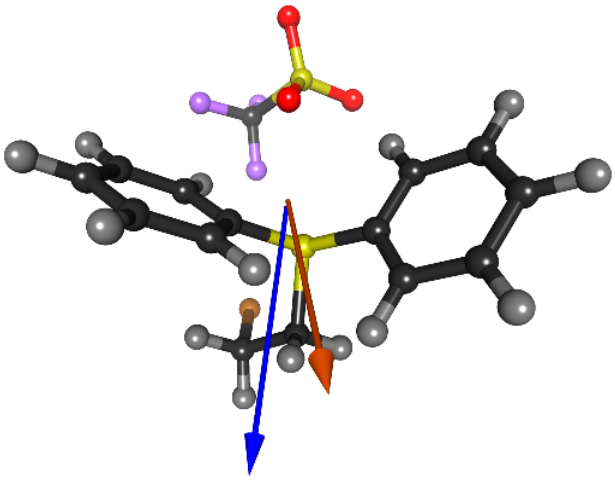

Figure 6: Total dipole moment for the BEST molecule computed from experimental (blue) and theoretical (red) models.

The dipolar charge distribution explaining the dipole moment orientation can also be seen on the electrostatic potential surfaces (Fig. 6), with a negative potential around the triflate anion. The value of the dipole moment for the Exp model is found to be 15% lower than the theoretical one. If the formal charges of the two ions were not constrained to be ±1, the contrary would be observed, in accordance with the fact that molecular dipole moments derived from

experimental charge density studies often present pronounced enhancements compared to independent theoretical estimates[41].

Conclusion.

An experimental charge density analysis of the compound bromoethylsulfonium triflate was performed as well as a high level *ab initio* periodic computation of the system. The analysis of the charge distribution on the basis of the Exp model did reveal very interesting results.

Generally, it is believed that the C13 atom being attached to a triply covalently bonded $S1^{+}$ atom is comparatively more electron deficient. So in this case, a base should preferentially abstract an acidic hydrogen from atom C13. The presence of the bromine atom adjacent to C14 renders the H14(A,B) hydrogen atoms also more acidic. The electrostatic potential at the molecular surface shows a strongly electropositive region around the sulphur atom, which is favourable to attract a nucleophile base. The electrostatic potential is also positive around the H14(A,B) hydrogen atoms compared to the H13(A,B) hydrogen atoms.

The distribution of charges raises again the question how the reaction actually proceeds. Previously Yar *et al.*[4] have indentified the *in situ* transformation of the bromoethyl sulfonium salt to vinyl sulfonium salt in the presence of a base. In this process, a base removes a proton from a carbon atom of the bromoethyl group, and then an elimination reaction occurs (the HBr group being removed).

The question raised by our study is whether the proton is removed from C14 or C13 atom. Most likely if H^{+} is removed from the C13 which is adjacent to the positively charged S1 atom, the carbanion would be more stable than if the proton is taken from the C14 atom, located next to the bromine atom.

A possibility remains that the proton extraction occurs first on C14, which holds more acidic hydrogen atoms according to the experimental electrostatic potential map. Then, the relative stability of the C14 and C13 carbanions being in favour of the second one, the C14 atom may be re-protonated by exchange with the neighbour atom C13. At this point, the C13 carbanion being stabilized by the $S1^{+}$ atom, no reverse protonation would take place. In particular, a possible perspective would be to analyze, in the same way, what the DVST vinyl homologue is producing *in situ* (Scheme 2).

Acknowledgements. M.A. thanks the Higher Education Commission of Pakistan for PhD funding.

Supporting Information Available:

Figures: plot of observed vs. expected residual electron density; plot of average Fobs / average Fcalc, residual and static electron density maps; Rfree plotted as a function of restraints weight; Hirshfeld surface; fingerprint plots of the Hirshfeld surface; molecular surface coloured according to ESP, after refinement without formal charge constraint on anion/cation. Tables: list of the bond and intermolecular critical points with topological properties. CIF file. This material is available free of charge via the Internet at http://pubs.acs.org.

References

(1) Unthank, M. G.; Hussain, N.; Aggarwal, V. K. *Angew Chemie Int. Edition* **2006**, *45*, 7066.

(2) Kokotos, C. G.; McGarrigle, E. M.; Aggarwal, V. K. *Synlett* **2008**, *2008*, 2191.

(3) Yar, M.; McGarrigle, E. M.; Aggarwal, V. K. *Angewandte Chemie International Edition* **2008**, *47*, 3784.

(4) Yar, M.; McGarrigle, E. M.; Aggarwal, V. K. *Organic Letters* **2009**, *11*, 257.

(5) Yar, M.; Unthank, M. G.; McGarrigle, E. M.; Aggarwal, V. K. *Chemistry – An Asian J.* **2011**, *6*, 372.

(6) Fritz, S. P.; Mumtaz, A.; Yar, M.; McGarrigle, E. M.; Aggarwal, V. K. *European J. Organic Chemistry* **2011**, *2011*, 3156.

(7) McGarrigle, E. M.; Fritz, S. P.; Favereau, L.; Yar, M.; Aggarwal, V. K. *Organic Letters* **2011**, *13*, 3060.

(8) von E. Doering, W.; Schreiber, K. C. *J. Am. Chem. Soc.* **1955**, *77*, 514.

(9) Wang, Y.; Zhang, W.; Colandrea, V. J.; Jimenez, L. S. *Tetrahedron* **1999**, *55*, 10659.

(10) Gosselck, J.; Béress, L.; Schenk, H. *Angewandte Chemie International Edition in English* **1966**, *5*, 596.

(11) Wijtmans, R.; Vink, M. K. S.; Schoemaker, H. E.; van Delft, F. L.; Blaauw, R. H.; Rutjes, F. P. J. T. *Synthesis* **2004**, *2004*, 641.

(12) Yar, M.; McGarrigle, E. M.; Aggarwal, V. K. In *Encyclopedia of Reagents for Organic Synthesis,*; John Wiley and Sons Ltd.: 2012.

(13) Agilent; Agilent Technologies Ltd: Yarnton, England, 2010.

(14) Clark, R. C.; Reid, J. S. *Acta Crystallogr. Section A* **1995**, *51*, 887.

(15) Blessing, R. H. Crystallogr. *Rev.* **1987**, *1*, 3.

(16) Zhurov, V. V.; Zhurova, E. A.; Pinkerton, A. A. *J. Applied Crystallogr.* **2008**, *41*, 340.

(17) Altomare, A.; Cascarano, G.; Giacovazzo, C.; Guagliardi, A. *J. Applied Crystallogr.* **1993**, *26*, 343.

(18) Sheldrick, G. *Acta Crystallogr., Sect. A* **2008**, *64*, 112.

(19) Jelsch, C.; Guillot, B.; Lagoutte, A.; Lecomte, C. *J. Applied Crystallogr.* **2005**, *38*, 38.

(20) Hansen, N. K.; Coppens, P. *Acta Crystallogr*. **1978.** A34, 909.

(21) Allen, F. *Acta Crystallogr. Section B.* **1986**, *42*, 515.

(22) Farrugia, L. *J. Applied Crystallogr.* **1997**, *30*, 565.

(23) R. Dovesi; V. R. S.; C. Roetti; R. Orlando; C. M. Zicovich-Wilson; F. Pascale; B. Civalleri; K. Doll; N. M. Harrison; I. J. Bush; P. D'Arco; M. Llunell, ; Version 1_0_2 ed.; University of Turin: Italy, 2008.

(24) Hohenberg, P.; Kohn, W. *Phys. Rev.* **1964**, *136*, 864.

(25) Lee, C.; Yang, W.; Parr, R. G. *Phys. Rev. B* **1988**, *37*, 785.

(26) Becke, A. D. *The J. Chemical Physics* **1993**, *98*, 5648.

(27) Hariharan, P. C.; Pople, J. A. *Theoret. Chim. Acta* **1973**, *28*, 213.

(28) Le Page, Y., Gabe, E. J. *Acta Crystallogr.* 1979. A**35**, 73-78

(29) Madsen, A. *J. Applied Crystallogr.* **2006**, *39*, 757.

(30) Stewart, R. *Acta Crystallogr.* **1976**, A*32*, 565.

(31) Zarychta, B.; Zaleski, J.; Kyziol, J.; Daszkiewicz, Z.; Jelsch, C. *Acta Crystallogr. Section B* **2011**, *67*, 250.

(32) Pillet, S. ; Souhassou, M. ; Lecomte, C. ; Schwarz, K. ; Blaha, P. ; Rérat, M.; Lichanot, A. ; Roversi, P. Acta Cryst. **2001**. A57, 290-303

(33) Coppens, P.; Guru Row, T. N.; Leung, P.; Stevens, E. D.; Becker, P. J.; Yang, Y. W. *Acta Crystallogr. Section A* **1979**, *35*, 63.

(34) Mette S. Schmøkel, M. S., Cenedese, S., Overgaard, J., Jørgensen, M. R. V., Chen, Y.-S., Gatti, C., Stalke, D. & Iversen, B. B. *Inorg. Chem*. **2012**, 51, 8607−8616.

(35) Love I. *J. Phys. Chem*. **2009**. 113, 2640-2646.

(36) Love I. *J. Phys. Chem*. **2006**. 110, 10507-10512.

(37) Bader, R. F. W. 1st ed.; Clarendon Press: Oxford, U.K, 1990; Vol. No. 22 in the International Series of Monographs on Chemistry.

(38) McKinnon, J. J.; Spackman, M. A.; Mitchell, A. S. *Acta Crystallogr.* **2004**. B60, 627.

(39) McKinnon, J. J.; Jayatilaka, D.; Spackman, M. A. *Chem. Commun***. 2007**, 3814.

(40) Desiraju G. R.; Steiner, T. IUCr Monographs on Crystallography, Vol. 9. Oxford: Oxford University Press/IUCr, 1999. The weak hydrogen bond in structural chemistry and biology.

(41) Spackman, M. A.. Munshi, P.. Dittrich, B. *Chem. Phys. Chem*. **2007**, 8, 2051.

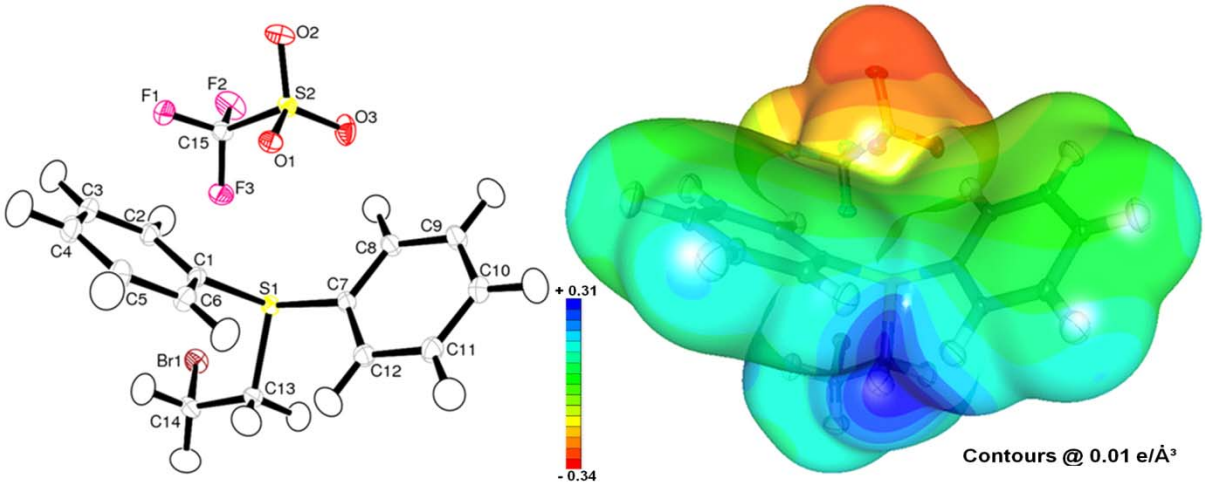

TOC Figure:

Left: *ORTEP* diagram of the BEST molecule showing the atom numbering scheme and the thermal ellipsoids (drawn at 50% probability level).

Right: 3D electron density surface coloured according to the electrostatic potential of the bromoethyl sulfonium cation.

Supplementary Materials.

Experimental and theoretical charge density analysis of a bromoethyl sulfonium salt.

Maqsood Ahmed, Muhammad Yar, Ayoub Nassour, Benoit Guillot, Claude Lecomte and Christian Jelsch.

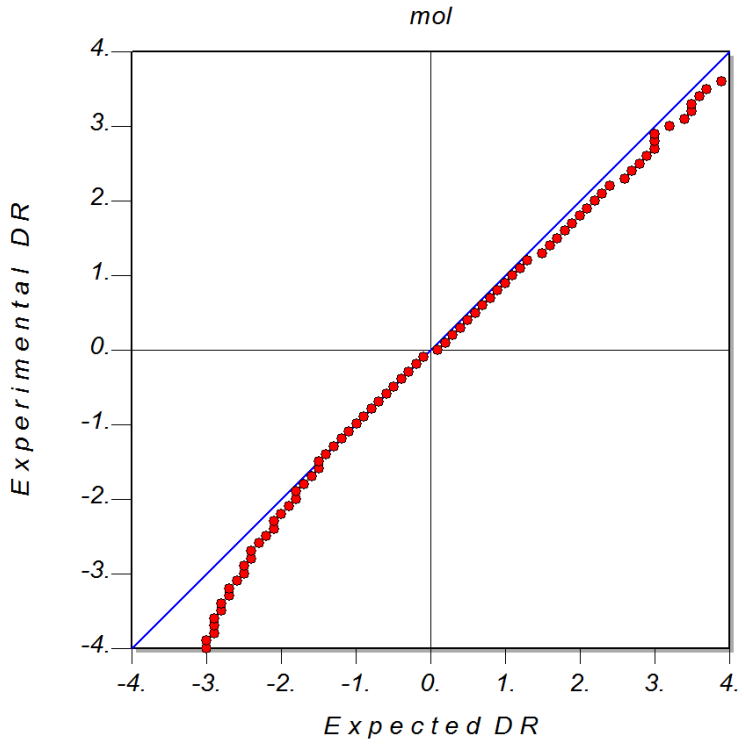

Figure Sup1. Expected and experimental residual density. Data are truncated at s<1Å^{-1}.

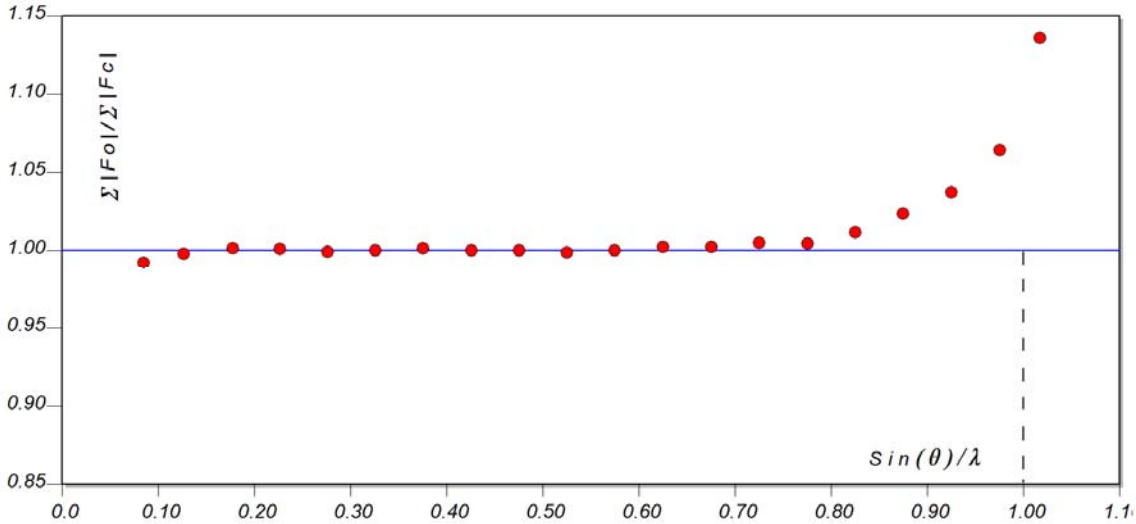

Figure Sup2. Average *F*obs / average *F*calc as a function of reciprocal resolution**.**

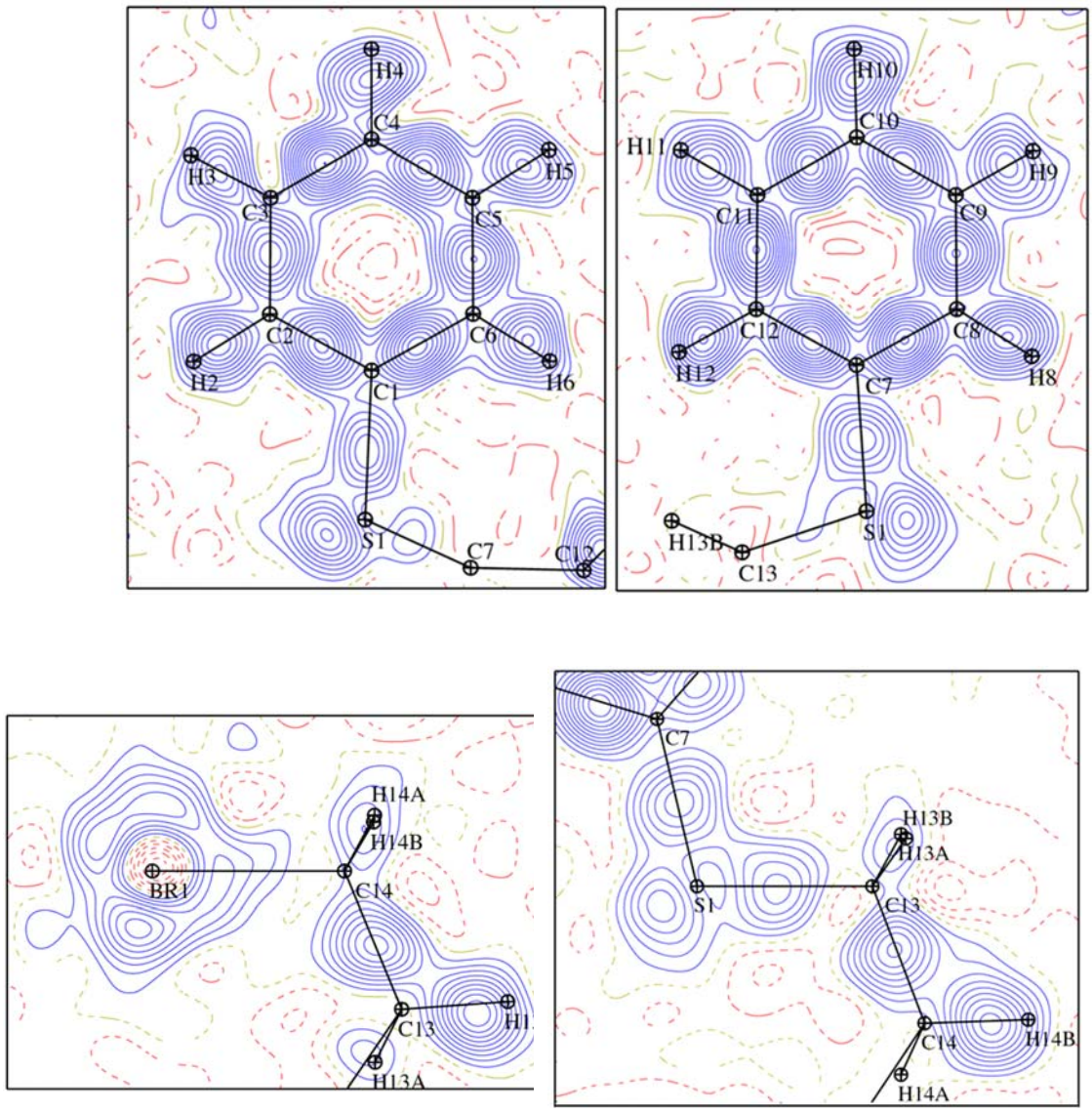

Figure Sup3.

Residual Fourier electron density on various parts of BEST molecule obtained after IAM experimental refinement. The contours are drawn at ±0.05 e/Å^3, positive and negative contours in blue and red, respectively. The reciprocal resolution is truncated at sinθ/λ <0.7 Å^{-1}.

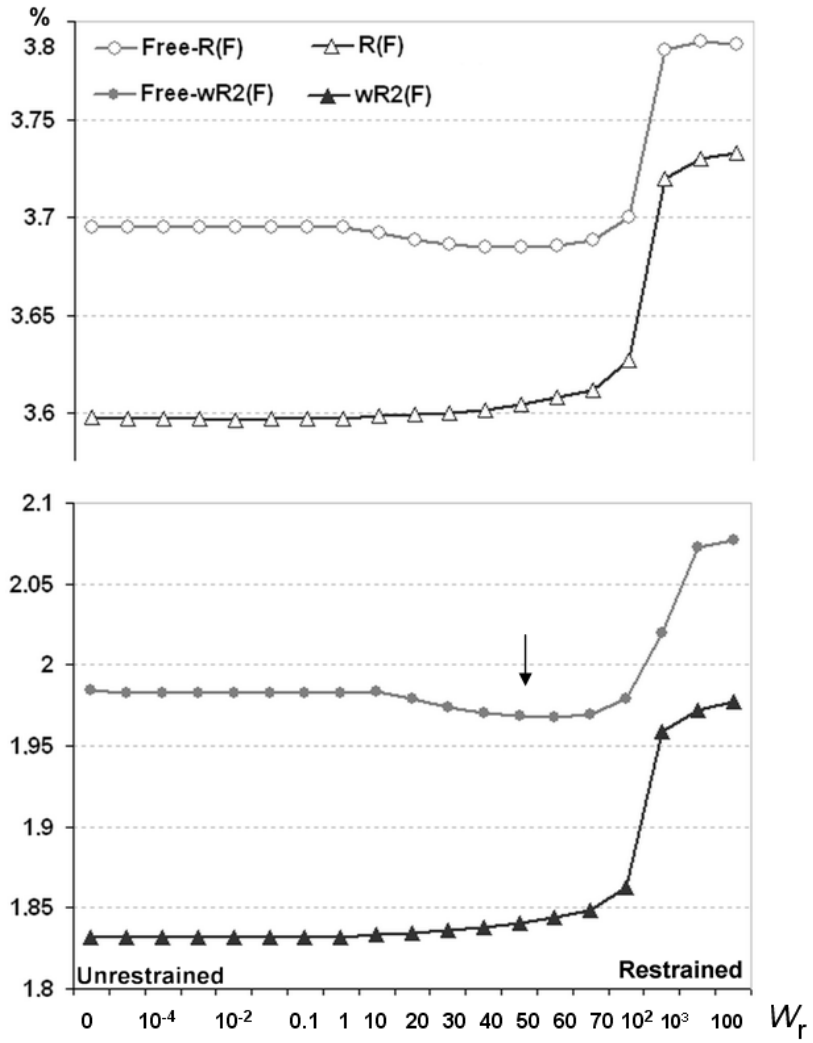

Figure Sup4:

Curves showing the statistical crystallographic indices evolution along the variation of weight applied on the charge density restraints (similarity and local symmetry). The optimal weight corresponding W=0.02 to the lowest free R factors was kept along the refinement.

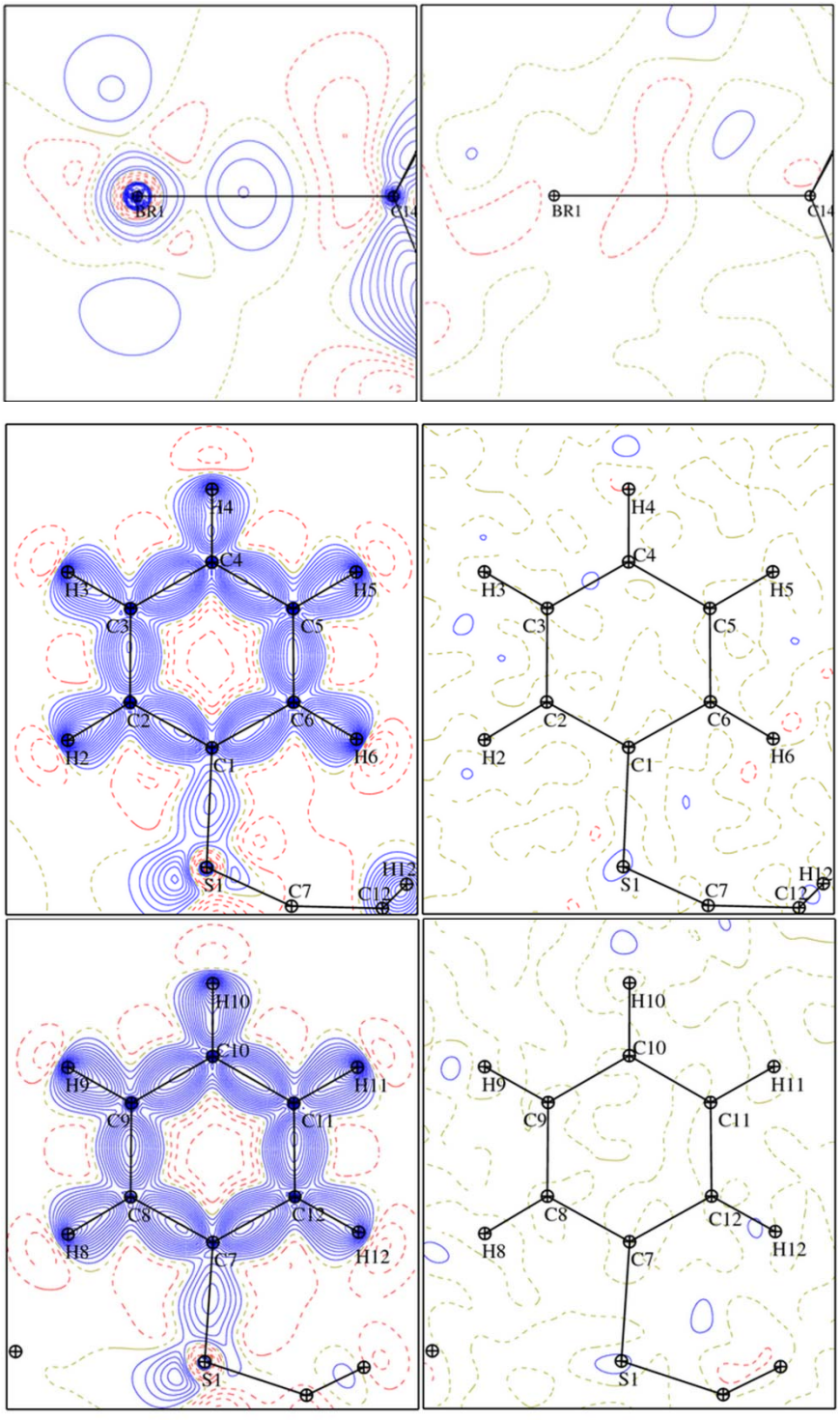

Figure Sup5: Experimental static deformation electron density (left) and Fourier residual electron densities (right) for the experimental multipolar model on the aromatic rings. Contour intervals are 0.05eÅ^{-3}; Blue solid lines are positive; red dot lines are negative; green dash line is a zero contour. The Fourier series have been truncated at $\sin\theta/\lambda$ <0.7 Å^{-1} for the computation of residual maps.

Figure Sup6:

Right:

Fingerprint plots of the Hirshfeld surface showing the proportion of major intermolecular interactions.

Left:

Hirshfeld surface of the BEST compound mapped with d_{norm} property showing the regions of interactions.

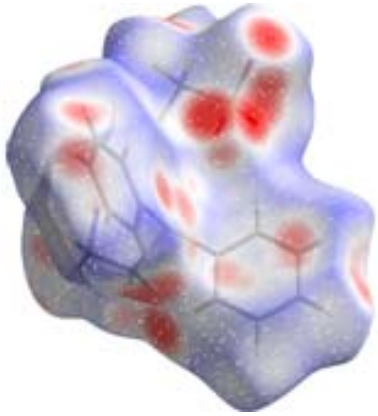

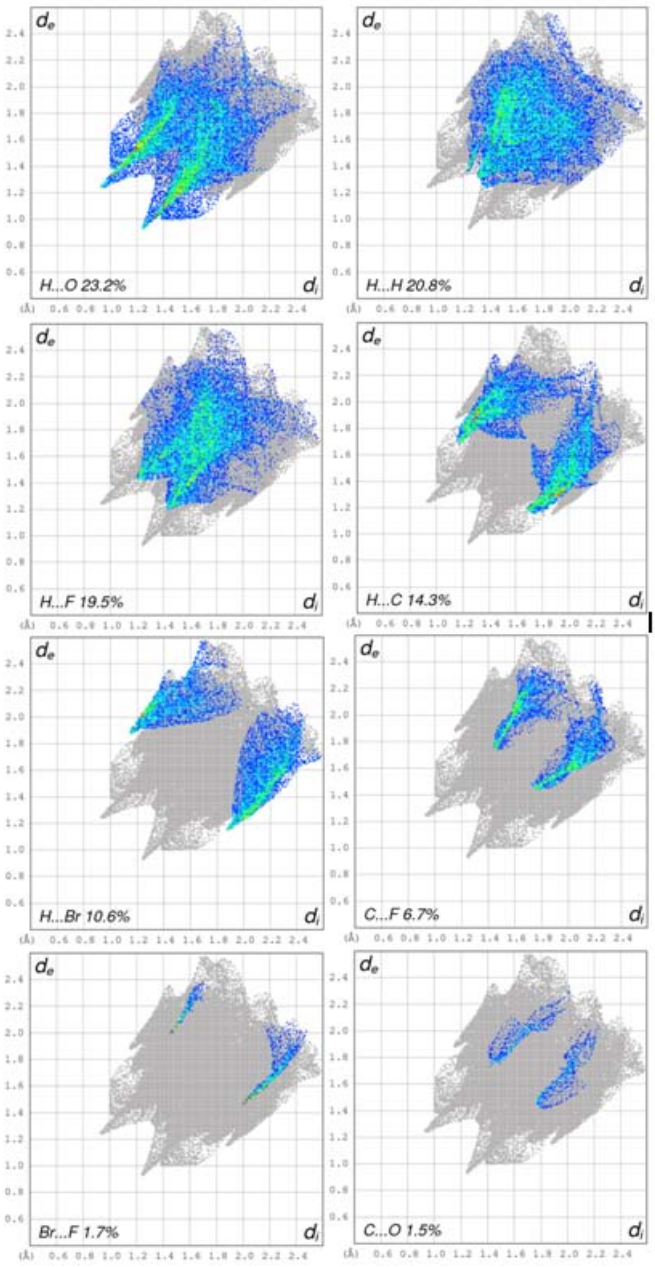

Figure Sup7.

Isosurface of static total electron density at ρ=0.01 e/Å^3 coloured according to the electrostatic potential generated by the BEST promolecule. The bromoethyl sulfonium moiety is in the foreground while the negatively charged triflate group is behind. The P_{val} valence populations were freely refined, with no ±1 e charge constraint on the cation and anion.

Properties are computed using

(a) experimental multipolar model (b) theoretical multipolar model.

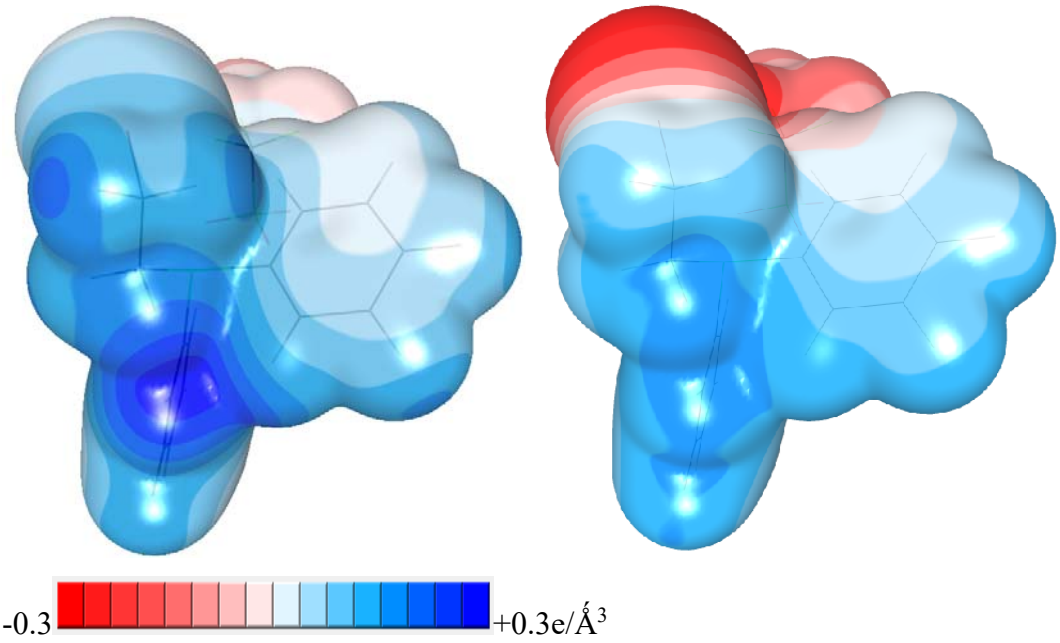

Table Sup1: List of the bond critical points and topological properties (see Table 5) of the BEST molecule. The values in upper/lower lines are from experiment/theory.

Bond	d_{12}	d_{1cp}	d_{2cp}	$\rho(\mathbf{r}_{cp})$	$\nabla^2\rho(\mathbf{r}_{cp})$	λ_1	λ_2	λ_3	ε
BR1-C14	1.9458(6)	1.0948	0.8513	0.9662	0.03	-4.60	-4.55	9.17	0.01
	1.9454	*1.0883*	*0.8572*	*0.8885*	*0.57*	*-4.01*	*-3.87*	*8.46*	*0.04*
S1-C1	1.7823(5)	0.9493	0.8330	1.2739	-5.70	-7.08	-6.71	8.09	0.05
	1.7813	*0.9741*	*0.8074*	*1.2719*	*-5.77*	*-6.81*	*-6.46*	*7.5*	*0.05*
S1-C7	1.7796(5)	0.9508	0.8291	1.2880	-5.52	-7.14	-6.89	8.51	0.04
	1.7789	*0.9783*	*0.8009*	*1.2631*	*-5.40*	*-6.81*	*-6.32*	*7.73*	*0.08*
S1-C13	1.8158(5)	0.9785	0.8372	1.1891	-4.49	-6.57	-6.06	8.14	0.08
	1.8149	*1.0117*	*0.8033*	*1.1773*	*-4.40*	*-6.27*	*-5.84*	*7.71*	*0.07*
S2-C15	1.8320(6)	0.8981	0.9341	1.3348	-9.24	-7.73	-7.55	6.03	0.02
	1.8329	*0.8018*	*1.0312*	*1.3112*	*-10.15*	*-6.01*	*-5.90*	*1.76*	*0.02*
S2-O1	1.4508(8)	0.5918	0.8591	2.1894	3.33	-14.89	-14.02	32.24	0.06
	1.4511	*0.5781*	*0.8732*	*1.9489*	*19.12*	*-10.82*	*-10.54*	*40.48*	*0.03*
S2-O2	1.4467(9)	0.5921	0.8552	2.1741	3.79	-14.41	-14.28	32.49	0.01
	1.4455	*0.5778*	*0.8681*	*1.9243*	*20.22*	*-10.71*	*-10.24*	*41.17*	*0.05*
S2-O3	1.4410(9)	0.5924	0.8503	2.2165	3.78	-14.39	-14.29	32.46	0.01
	1.4398	*0.5752*	*0.8648*	*2.0058*	*20.41*	*-11.47*	*-11.1*	*42.98*	*0.03*
F1-C15	1.3415(6)	0.8238	0.5180	1.9470	-15.61	-15.92	-15.20	15.50	0.05
	1.3442	*0.8146*	*05302*	*1.8995*	*-15.19*	*-15.13*	*-13.45*	*13.39*	*0.13*
F2-C15	1.3334(7)	0.8263	0.5074	1.9328	-13.94	-15.15	-14.18	10.37	0.06
	1.3309	*0.8157*	*0.5152*	*1.9687*	*-18.56*	*-16.36*	*-14.93*	*12.73*	*0.10*
F3-C15	1.3340(6)	0.8236	0.5109	1.9784	-16.23	-16.35	-15.25	15.36	0.07
	1.3340	*0.8077*	*0.5269*	*2.0195*	*-13.61*	*-16.35*	*-14.54*	*17.28*	*0.11*
C1-C2	1.3911(4)	0.7146	0.6766	2.1410	-18.64	-16.19	-13.65	11.20	0.16
	1.3917	*0.7073*	*0.6846*	*2.0855*	*-17.95*	*-14.98*	*-12.4*	*9.43*	*0.21*
C1-C6	1.3911(7)	0.7085	0.6828	2.1426	-18.80	-16.55	-13.55	11.30	0.18
	1.3922	*0.7153*	*0.677*	*2.0816*	*-17.92*	*-14.83*	*-12.39*	*9.3*	*0.20*
C2-C3	1.3948(7)	0.6848	0.7101	2.0993	-17.89	-15.62	-13.20	10.92	0.15
	1.3968	*0.6943*	*0.7025*	*2.0737*	*-17.48*	*-15.0*	*-12.61*	*10.12*	*0.19*
C3-C4	1.3925(9)	0.6702	0.7223	2.1798	-19.37	-17.10	-14.09	11.82	0.18
	1.3937	*0.6818*	*0.712*	*2.0912*	*-18.19*	*-15.23*	*-12.8*	*9.83*	*0.19*
C4-C5	1.3919(8)	0.7228	0.6691	2.1769	-19.83	-17.05	-14.19	11.41	0.17
	1.3916	*0.6865*	*0.7051*	*2.0982*	*-18.57*	*-15.29*	*-12.86*	*9.57*	*0.19*
C5-C6	1.3917(7)	0.6891	0.7027	2.1351	-19.06	-16.44	-13.40	10.78	0.19
	1.3930	*0.6824*	*0.7106*	*2.0793*	*-17.85*	*-14.99*	*-12.59*	*9.73*	*0.19*
C7-C8	1.3955(6)	0.7136	0.6821	2.1295	-18.44	-16.18	-13.70	11.44	0.15
	1.3966	*0.715*	*0.6818*	*2.0722*	*-17.7*	*-14.77*	*-12.29*	*9.35*	*0.20*
C7-C12	1.3933(6)	0.7140	0.6794	2.1401	-18.36	-16.60	-13.51	11.75	0.19

	1.3940	*0.7139*	*0.6802*	*2.0648*	*-17.49*	*-14.66*	*-12.29*	*9.46*	*0.19*
C8-C9	1.3936(7)	0.6945	0.6991	2.1112	-18.34	-15.71	-13.32	10.69	0.15
	1.3936	*0.7032*	*0.6904*	*2.0802*	*-17.90*	*-15.04*	*-12.62*	*9.76*	*0.19*
C9-C10	1.3920(7)	0.6830	0.7090	2.1457	-18.59	-16.47	-13.48	11.35	0.18
	1.3911	*0.7075*	*0.6836*	*2.0909*	*-18.25*	*-15.28*	*-12.79*	*9.82*	*0.19*
C10-C11	1.3925 (7)	0.7024	0.6901	2.1873	-19.72	-17.20	-14.37	11.86	0.16
	1.3923	0.7094	0.6829	2.0837	-18.07	-15.23	-12.75	9.92	0.19
C11-C12	1.3917 (7)	0.7049	0.6868	2.1500	-19.17	-16.60	-13.89	11.32	0.16
	1.3941	*0.7017*	*0.6924*	*2.0804*	*-17.65*	*-15.09*	*-12.63*	*10.07*	*0.19*
C13-C14	1.5126(7)	0.7855	0.7278	1.6641	-10.22	-11.16	-10.69	11.62	0.04
	1.5144	*0.7615*	*0.7534*	*1.6278*	*-9.46*	*-10.6*	*-10.24*	*11.37*	*0.04*
C2-H2	1.0823	0.7352	0.3771	1.8119	-16.79	-17.36	-16.61	17.19	0.04
	1.0069	*0.6636*	*0.3435*	*1.8942*	*-17.26*	*-17.96*	*-17.47*	*18.15*	*0.03*
C3-H3	1.0823	0.7335	0.3489	1.7585	-15.84	-16.77	-16.23	17.15	0.03
	1.0278	*0.6729*	*0.3549*	*1.8789*	*-17.2*	*-17.75*	*-17*	*17.55*	*0.04*
C4-H4	1.0829	0.7317	0.3511	1.8229	-17.39	-18.06	-17.16	17.83	0.05
	1.0398	*0.6809*	*0.3589*	*1.8809*	*-17.67*	*-17.68*	*-17.04*	*17.06*	*0.04*
C5-H5	1.0826	0.7307	0.3519	1.7777	-16.24	-17.05	-16.20	17.01	0.05
	1.0287	*0.6747*	*0.3541*	*1.8782*	*-17.46*	*-17.65*	*-17.05*	*17.24*	*0.04*
C6-H6	1.0822	0.7335	0.3487	1.8199	-17.68	-17.79	-16.66	16.77	0.06
	1.0071	*0.6662*	*0.3409*	*1.9019*	*-17.55*	*-18.19*	*-17.42*	*18.05*	*0.04*
C8-H8	1.0826	0.7312	0.3515	1.8272	-17.46	-17.53	-16.59	16.67	0.05
	1.0054	*0.6663*	*0.3391*	*1.9081*	*-17.71*	*-18.35*	*-17.61*	*18.25*	*0.04*
C9-H9	1.0822	0.7284	0.3539	1.7731	-15.94	-16.69	-16.08	16.83	0.04
	1.0155	*0.6612*	*0.3545*	*1.8811*	*-17.32*	*-17.66*	*-16.93*	*17.27*	*0.04*
C10-H10	1.0822	0.7280	0.3542	1.8427	-17.22	-17.95	-17.29	18.01	0.04
	1.0117	*0.6771*	*0.3346*	*1.8968*	*-16.95*	*-18.47*	*-17.87*	*19.4*	*0.03*
C11-H11	1.0823	0.7330	0.3493	1.8147	-16.73	-17.63	-16.89	17.79	0.04
	1.0257	*0.6707*	*0.355*	*1.8745*	*-17.14*	*-17.65*	*-16.89*	*17.54*	*0.04*
C12-H12	1.0823	0.7404	0.3420	1.8048	-17.55	-17.69	-16.88	17.02	0.05
	1.0067	*0.6696*	*0.3373*	*1.9015*	*-17.26*	*-18.39*	*-17.7*	*18.93*	*0.04*
C13-H13A	1.0907	0.7393	0.3515	1.7932	-15.92	-17.02	-17.01	18.11	0.00
	1.0023	*0.6775*	*0.3249*	*1.896*	*-16.77*	*-18.46*	*-18.35*	*20.03*	*0.01*
C13-H13B	1.0914	0.7309	0.3606	1.7418	-14.87	-16.25	-16.22	17.60	0.00
	1.0224	*0.6783*	*0.3442*	*1.8445*	*-15.32*	*-17.22*	*-17.01*	*18.91*	*0.01*
C14-H14A	1.0914	0.7338	0.3577	1.8048	-16.52	-16.68	-16.51	16.67	0.01
	1.0480	*0.6902*	*0.3579*	*1.8453*	*-16.07*	*-17.05*	*-16.65*	*17.63*	*0.02*
C14-H14B	1.0919	0.7308	0.3611	1.7789	-15.89	-16.30	-16.08	16.48	0.01
	1.0536	*0.6987*	*0.3549*	*1.8482*	*-16.55*	*-17.13*	*-16.98*	*17.56*	*0.01*

Table Sup2: List of intermolecular CPs and topological properties. The upper line stands for the experimental and the lower line stands for the theoretical values. d_{12} is the interatomic distances, d_{1cp} and d_{2cp} (Å) are the distance between the first / second atom and the CP; $\rho(r_{cp})$ is the electron density (e.Å^{-3}); $\nabla^2\rho(r_{cp})$ is the Laplacian (e.Å^{-5}); λ_1, λ_2, λ_3 are the eigenvalues of Hessian matrix (e.Å^{-5}); ε the ellipticity whereas ***G*** and ***V*** denote the kinetic and potential energies, respectively. The symmetry codes are the following:

(i) *-X+2; -Y ; -Z+1* (ii) *-X+1 ; -Y ; -Z+1* (iii) *X+1/2 ; -Y-1/2 ; Z-1/2*
(iv) *-X+3/2 ; Y-1/2 ; -Z+3/2* (v) *X-1/2 ; -Y-1/2 ; Z-1/2* (vi) *X-1/2 ; -Y-1/2 ; Z+1/2*
(vii) *X ; Y-1 ; Z* (viii) *X+1 ; Y ; Z* (ix) *X-1 ; Y ; Z*
(x) *-X+2 ; -Y ; -Z+2* (xi) *-X+1 ; -Y ; -Z+2* (xii) *-X+3/2 ; Y+1/2 ; -Z+3/2*

Bond Path	D_{12}	d_{1cp}	D_{2cp}	$\rho(\mathbf{r}_{CP})$	$\nabla^2\rho$ $(\mathbf{r}_{CP})$	λ_1	λ_2	λ_3	ε	$\boldsymbol{G}$ $(\mathbf{r}_{CP})$	$\boldsymbol{V}$ $(\mathbf{r}_{CP})$
Br1^{i}···H3	3.2170	1.175	2.0538	0.021	0.32	-0.05	-0.05	0.42	0.03	6.37	-3.95
	3.2717	1.2207	2.0532	0.027	0.34	-0.07	-0.06	0.47	0.05	6.97	-4.59
Br1···H9^{ii}	3.1996	1.5056	1.7318	0.03	0.45	-0.07	-0.04	0.57	0.41	9.04	-5.89
	3.0835	1.8949	1.1965	0.042	0.46	-0.11	-0.1	0.66	0.08	9.97	-7.4
S2^{iii}···H5	-	-	-	-	-	-	-	-	-	-	-
	3.7578	1.3177	2.5265	0.026	0.41	-0.07	-0.05	0.53	0.29	8.07	-5.07
F1···C3^{i}	3.1933(1)	1.5181	1.6778	0.03	0.45	-0.06	-0.05	0.56	0.27	9.06	-5.88
	3.1935	1.5184	1.6779	0.03	0.46	-0.07	-0.04	0.57	0.34	9.28	-5.98
F1···H9^{iii}	2.8465	1.5253	1.3734	0.027	0.44	-0.06	-0.03	0.53	0.49	8.83	-5.53
	2.8685	1.5409	1.335	0.026	0.44	-0.07	-0.04	0.55	0.39	8.77	-5.47
F1···H10^{iii}	2.6679	1.4806	1.2119	0.037	0.62	-0.21	-0.11	0.48	0.07	12.51	-8.19
	2.7031	1.466	1.2443	0.036	0.59	-0.11	-0.01	0.8	0.14	11.98	-7.81
F1···H11^{iv}	2.9396	1.6444	1.3442	0.013	0.24	-0.03	-0.03	0.31	0.03	4.62	-2.64
	2.9774	1.6267	1.3601	0.015	0.26	-0.04	-0.04	0.33	0.04	4.96	-2.89
F2···C11^{ii}	3.5909(6)	1.6464	1.989	0.016	0.23	-0.03	-0.01	0.27	0.5	4.45	-2.28
	3.5997	1.6512	2.0015	0.015	0.22	-0.03	-0.01	0.27	0.54	4.31	-2.59
F2···H4^{v}	2.6304	1.4802	1.1826	0.034	0.59	-0.11	-0.1	0.8	0.06	11.85	-7.59
	2.6464	*1.4676*	*1.1969*	*0.034*	*0.58*	*-0.11*	*-0.1*	*0.79*	*0.07*	*11.76*	*-7.59*
F2^{vi}···H9	2.6751	1.2102	1.4951	0.027	0.48	-0.08	-0.06	0.62	0.27	9.51	-5.88
	2.7186	1.225	1.4985	0.031	0.52	-0.1	-0.08	0.7	0.19	10.42	-6.63
F3···C9^{ii}	3.1996	1.5056	1.7318	0.03	0.45	-0.07	-0.04	0.57	0.41	9.04	-5.89
	3.2038	1.5131	1.7176	0.03	0.45	-0.07	-0.04	0.57	0.36	9.12	-5.89
F3···H3^{i}	2.7857	1.5019	1.3387	0.03	0.48	-0.08	-0.07	0.62	0.16	9.56	-6.12
	2.8114	1.5068	1.3412	0.03	0.49	-0.09	-0.07	0.64	0.26	9.82	-6.3
O1···H6^{iv}	2.3965	1.4653	0.969	0.068	1.08	-0.23	-0.13	1.45	0.43	23.15	-16.9
	2.454	1.4216	1.044	0.072	1.08	-0.25	-0.16	1.49	0.34	23.59	-17.7
O1···H12^{iv}	2.3115	1.4035	0.9319	0.066	1.17	-0.23	-0.23	1.64	0.01	24.7	-17.4
	2.3772	1.3798	1	0.08	1.18	-0.29	-0.28	1.75	0	26	-20
O1···H13B^{iv}	2.7378	1.6246	1.1305	0.021	0.44	-0.05	-0.03	0.52	0.37	8.45	-4.95
	-	-	-	-	-	-	-	-	-	-	-
O2···H4^{v}	2.6611	1.5393	1.1636	0.042	0.63	-0.12	-0.1	0.85	0.13	13	-8.87
	2.6871	*1.5452*	*1.1681*	*0.043*	*0.61*	*-0.13*	*-0.1*	*0.85*	*0.23*	*12.77*	*-8.83*
O2···H5^{v}	-	-	-	-	-	-	-	-	-	-	-
	2.9108	1.6174	1.3163	0.026	0.41	-0.07	-0.05	0.53	0.27	8.11	-5.1
O2···H10^{iii}	2.6927	1.6173	1.0852	0.021	0.48	-0.06	-0.05	0.59	0.16	9.19	-5.53
	2.7593	1.5679	1.1916	0.032	0.49	-0.1	-0.1	0.69	0.01	9.94	-6.47
O2···H14B^{vii}	2.4835	1.4693	1.0368	0.044	0.77	-0.14	-0.13	1.05	0.06	15.69	-10.4

	2.5089	1.4657	1.0539	0.048	0.8	-0.16	-0.14	1.1	0.11	16.4	-11.1
O3···H13A^{ii}	2.1515	1.2897	0.8776	0.107	1.72	-0.42	-0.4	2.54	0.03	38.8	-30.8
	2.2214	1.2929	0.9308	0.118	1.64	-0.47	-0.42	2.52	0.1	38.56	-32.5
C3···H12^{iv}	3.2419	1.8588	1.391	0.02	0.24	-0.04	-0.03	0.31	0.31	4.9	-3.14
	3.2664	1.8935	1.3846	0.022	0.26	-0.05	-0.02	0.33	0.55	5.24	-3.42
C5···H9 ^{viii}	3.4745	2.0274	1.5307	0.012	0.15	-0.02	-0.01	0.18	0.44	2.9	-1.76
	3.5011	2.0161	1.5179	0.012	0.14	-0.02	-0.01	0.18	0.47	2.76	-1.67
C5···H13A^{iv}	2.8674	1.7623	1.3063	0.038	0.44	-0.08	-0.04	0.56	0.53	9.35	-6.69
	2.9153	1.7128	1.2907	0.038	0.45	-0.09	-0.04	0.58	0.51	9.49	-6.79
C6···H14B^{iv}	3.0656	1.7932	1.289	0.029	0.36	-0.07	-0.04	0.46	0.47	7.36	-4.94
	3.0839	1.8253	1.2603	0.028	0.36	-0.07	-0.05	0.48	0.34	7.29	-4.83
C9···H14A^{iv}	2.8695	1.7792	1.2183	0.038	0.47	-0.09	-0.04	0.59	0.53	9.83	-6.96
	2.8986	1.7526	1.2147	0.039	0.46	-0.09	-0.05	0.6	0.51	9.81	-7.0
C8···H13B^{iv}	-	-	-	-	-	-	-	-	-	-	-
	3.3925	1.9628	1.4783	0.015	0.19	-0.02	-0.01	0.22	0.47	3.71	-2.28
C10···H4^{ix}	3.5638	2.2258	1.3704	0.005	0.11	-0.01	-0.01	0.12	0.47	2.01	-1.07
	-	-	-	-	-	-	-	-	-	-	-
H2···H3^{i}	2.6434	1.3393	1.3496	0.017	0.25	-0.04	-0.04	0.34	0.03	4.91	-2.95
	2.7282	1.3822	1.3543	0.019	0.26	-0.05	-0.04	0.35	0.07	5.13	-3.19
H5···H5^{x}	2.9306	1.4662	1.4645	0.005	0.11	-0.01	0	0.13	0.68	2.08	-1.12
	3.011	1.5061	1.5046	0.008	0.12	-0.02	-0.01	0.15	0.22	2.25	-1.26
H10···H11^{xi}	2.7752	1.4475	1.3864	0.02	0.27	-0.05	-0.05	0.36	0.05	5.34	-3.38
	2.8288	1.4446	1.4019	0.021	0.27	-0.05	-0.04	0.36	0.16	5.34	-3.43
H14B···C12^{xii}	-	-	-	-	-	-	-	-	-	-	-
	3.0279	1.2841	1.8436	0.032	0.038	-0.07	-0.02	0.47	0.65	7.85	-5.4
H14B···H6^{xii}	2.5928	1.2889	1.5556	0.029	0.36	-0.07	-0.04	0.46	0.47	7.36	-4.94
	2.6459	1.2602	1.4889	0.028	0.36	-0.07	-0.05	0.48	0.34	7.29	-4.83

Table Sup3. Zeta and N_l exponents of Slater functions used for the multipolar description of atoms.

atom	zeta	N_l			
atom	(bohr^{-1})	DIP	QUA	OCT	HEX
H	2.000	1			
C	3.176	2	2	3	
O	4.466	2	2	3	
F	5.108	2	2	3	
S	3.851	4	4	6	8
Br	4.732	6	6	6	6